Supplement of Biogeosciences, 22, 1427–1446, 2025
https://doi.org/10.5194/bg-22-1427-2025-supplement

Biogeosciences Open Access EGU

Supplement of

A microbially driven and depth-explicit soil organic carbon model constrained by carbon isotopes to reduce parameter equifinality

Marijn Van de Broek et al.

Correspondence to: Marijn Van de Broek (marijn.vandebroek@usys.ethz.ch)

Supplementary information

Contents

S1 Detailed description of soilcarb

The R codes can be downloaded from doi.org/10.5281/zenodo.14592264.

S1.1 Spatial and temporal resolution and units

SOILcarb (**S**imulation of **O**rganic carbon and its **I**sotopes by **L**inking **ca**rbon dynamics in the **r**hizosphere and **b**ulk soil) is a depth-explicit soil organic carbon (SOC) model. It simulates dynamics of ^{12}C, ^{13}C and ^{14}C along the soil profile using either a fixed or variable layer thickness. The model used in the present manuscript uses a variable layer thickness, being calculated as:

$$dz_i = dz_{i-1} + (dz_{i-1} \cdot f_b) \qquad \text{for } i > 1 \tag{S1}$$

where dz_i is the layer thickness if the i^{th} layer (m) and f_b is a factor regulating the increase in layer thickness with depth (unitless). The thickness of the uppermost soil layer (dz_1) has to be provided by the user, and was 0.01 m in the present study. In the present article, SOILcarb simulates depth profiles of organic carbon (OC) down to 1 m depth. Model inputs are provided with an annual time step, assuming that all model parameters remain constant within a given year. SOILcarb has been programmed in R (R Core Team, 2024), with the differential equations regulating the flows of carbon in the model (see below) being solved using the *lsodes* solver from the DeSolve package (Soetaert et al., 2010). It is noted that the model can be adapted to perform calculations at a daily time step. The model is run for a soil surface area of 1 m^2, with the amount of OC in every depth layer being expressed as kg C m^{-2} for the depth of the respective layer.

S1.2 General model structure

In SOILcarb, OC cycling is performed in three conceptual compartments: the litter layer, the rhizosphere and the bulk soil, with every compartment having a separate microbial community ($C_{mic\text{-}l}$, $C_{mic\text{-}r}$ and $C_{mic\text{-}b}$ for the litter layer, rhizosphere and bulk soil, respectively) (Figure S1). Carbon is transferred from the litter layer to the mineral soil through bioturbation of particulate OC (POC; $C_{POC\text{-}l}$) or leaching of dissolved OC (DOC; $C_{DOC\text{-}l}$). The rhizosphere is the part of the model where OC cycles rapidly, as this is the zone in the soil where root exudates provide microbes with ample substrate. In SOILcarb, root exudates enter the soil in the bio-available carbon pool ($C_{bioav\text{-}r}$), while inputs from dead roots enter the POC pool ($C_{POC\text{-}r}$). The bulk soil compartment receives carbon inputs from (i) leached litter DOC, (ii) the non-dissolvable portion of microbial necromass from microbes in the rhizosphere and (iii) a fixed portion of $C_{bioav\text{-}r}$. The latter flux allows the direct adsorption of plant-derived OC onto soil minerals. This OC enters the DOC pool in the bulk soil ($C_{DOC\text{-}b}$). There, OC cycles much slower compared to the rhizosphere due to the protection of OC by adsorption on soil minerals ($C_{min\text{-}b}$). A portion of substrate taken up by microbes is lost as CO_2 based on a fixed carbon use efficiency (CUE). In addition, microbes take up a portion of carbon through heterotrophic CO_2 assimilation. Leaching of $C_{bioav\text{-}r}$ and $C_{DOC\text{-}b}$ is simulated as an advective process, bioturbation of $C_{POC\text{-}r}$, $C_{DOC\text{-}b}$, $C_{min\text{-}b}$ and $C_{mic\text{-}b}$ is simulated as a diffusive process.

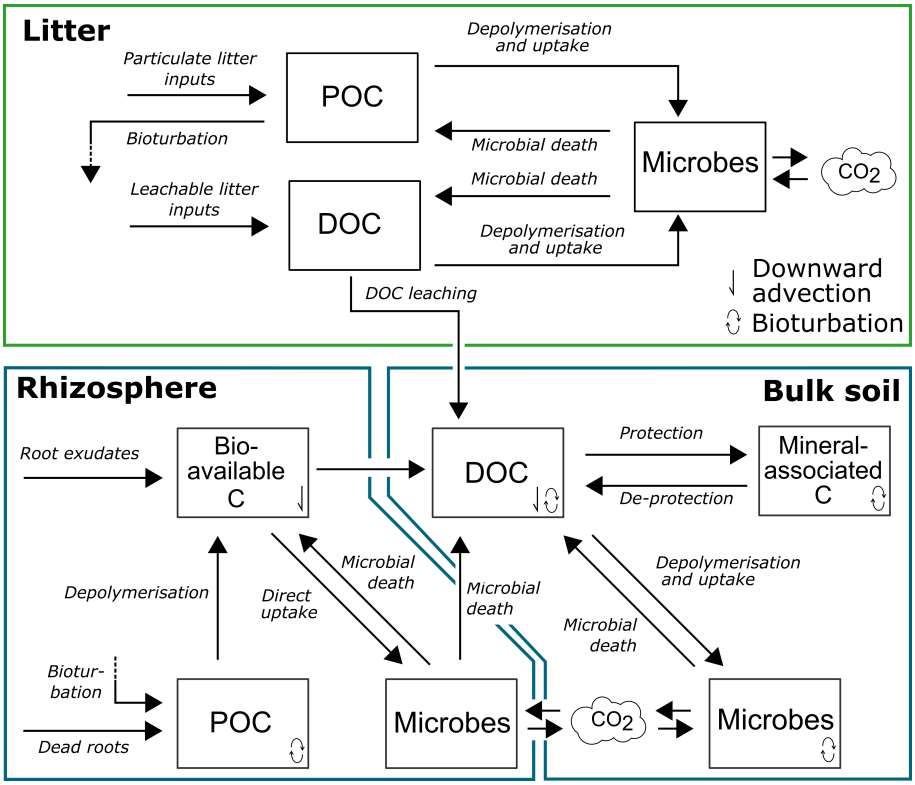

Figure S1. Conceptual model of SOILcarb showing the model pools and fluxes of organic carbon in the litter layer, rhizosphere and bulk soil. *POC* = particulate organic matter; *DOC* = dissolvable organic matter.

S1.3 Model equations

The equations below describe the fluxes of total OC. In the model, however, OC fluxes are calculated separately for ^{12}C, ^{13}C and ^{14}C following the same equations, as described in section S1.6.

S1.3.1 Litter layer

Litter carbon inputs. Carbon inputs to the litter layer are distributed over the particulate OC ($C_{POC\text{-}l}$) and dissolvable OC ($C_{DOC\text{-}l}$) pools:

$$F_{t,DOC-l} = f_{leachable} \cdot i_{litter} \quad \text{(S2)}$$

$$F_{t,POC-l} = (1 - f_{leachable}) \cdot i_{litter} \quad \text{(S3)}$$

Where $F_{t,DOC\text{-}l}$ is the input of OC into the litter DOC pool in year t (kg C m^{-2} yr^{-1}), $F_{t,POC\text{-}l}$ is the input of OC into the litter POC pool in year t (kg C m^{-2} yr^{-1}), $f_{leachable}$ is the fraction leachable OC of total litter inputs (unitless) and i_{litter} is the total

amount of annual litter OC inputs (kg C m^{-2} yr^{-1}).

Litter OC depolymerisation and microbial uptake. Both $C_{DOC\text{-}l}$ and $C_{POC\text{-}l}$ are depolimerized and taken up by litter microbes ($C_{mic\text{-}l}$) in a single-step process. This competition for $C_{DOC\text{-}l}$ and $C_{POC\text{-}l}$ is simulated using the equilibrium chemistry approximation (ECA) (Tang and Riley, 2013):

$$F_{POC-l\rightarrow mic-l} = V_{max\_POC-l}\frac{C_{POC-l}\cdot C_{mic-l}}{K_{m\_POC-l}\cdot(1+\frac{C_{POC-l}}{K_{m\_POC-l}}+\frac{C_{DOC-l}}{K_{m\_DOC-l}})+C_{mic-l}}\cdot(1-\alpha)\cdot CUE\_l \quad \text{(S4)}$$

$$F_{DOC-l\rightarrow mic-l} = V_{max\_DOC-l}\frac{C_{DOC-l}\cdot C_{mic-l}}{K_{m\_DOC-l}\cdot(1+\frac{C_{POC-l}}{K_{m\_POC-l}}+\frac{C_{DOC-l}}{K_{m\_DOC-l}})+C_{mic-l}}\cdot(1-\alpha)\cdot CUE\_l \quad \text{(S5)}$$

Where V_{max_l} is the maximum fraction of the POC and DOC litter pools that can be depolymerized and taken up by microbes (yr^{-1}), $C_{mic\text{-}l}$ is the size of the litter microbial biomass pool (kg C m^{-2}), $K_{m\_DOC\text{-}l}$ and $K_{m\_POC\text{-}l}$ are the affinities (similar to half saturation constants, i.e. the mass of litter microbes at which the depolymerisation rate is 50 % of V_{max}; kg C m^{-2}) and *CUE_l* is the microbial carbon use efficiency. The amount of carbon taken up by microbes from litter carbon is reduced by the factor (1 – α), with α being the fraction of microbial carbon uptake coming from heterotrophic CO_2 assimilation. The value of α was fixed at 0.011, based on previous research at Hainich forest (Akinyede et al., 2020), where the simulated soil profile in the present manuscript is located. It is noted that values of α up to 0.05 have been reported for other ecosystems (Nel and Cramer, 2019; Šantrůčková et al., 2018, 2005; Miltner et al., 2004). The amount of carbon taken up from $^{12}CO_2$, $^{13}CO_2$ and $^{14}CO_2$ from the atmosphere (litter microbes) or from soil gas (soil microbes) is being corrected for ratios of $^{13}C/^{12}C$ and $^{14}C/^{12}C$ of atmospheric and soil CO_2-C of the simulated year. The simulation of the $\delta^{13}C$ and $\Delta^{14}C$ value of CO_2 in the soil atmosphere is described in section S1.4. The amount of heterotrophic CO_2-C fixation by litter microbes is formulated as follows:

$$F_{CO_2-C\rightarrow mic} = (V_{max\_POC-l}\frac{C_{POC-l}\cdot C_{mic-l}}{K_{m\_POC-l}\cdot(1+\frac{C_{POC-l}}{K_{m\_POC-l}}+\frac{C_{DOC-l}}{K_{m\_DOC-l}})+C_{mic-l}}+ V_{max\_DOC-l}\frac{C_{DOC-l}\cdot C_{mic-l}}{K_{m\_DOC-l}\cdot(1+\frac{C_{POC-l}}{K_{m\_POC-l}}+\frac{C_{DOC-l}}{K_{m\_DOC-l}})+C_{mic-l}})\cdot\alpha\cdot CUE\_l \quad \text{(S6)}$$

Litter CO_2 respiration. The amount of carbon respired by microbes in the litter layer is calculated by multiplying the amount of OC uptake with 1 minus the carbon use efficiency:

$$F_{C_{mic-l}\rightarrow CO_2-C} = (V_{max\_POC-l}\frac{C_{POC-l}\cdot C_{mic-l}}{K_{m\_POC-l}\cdot(1+\frac{C_{POC-l}}{K_{m\_POC-l}}+\frac{C_{DOC-l}}{K_{m\_DOC-l}})+C_{mic-l}}+ V_{max\_DOC-l}\frac{C_{DOC-l}\cdot C_{mic-l}}{K_{m\_DOC-l}\cdot(1+\frac{C_{POC-l}}{K_{m\_POC-l}}+\frac{C_{DOC-l}}{K_{m\_DOC-l}})+C_{mic-l}})\cdot(1-CUE\_l) \quad \text{(S7)}$$

Microbial turnover in the litter layer. Microbial death is simulated following a logistic growth model (also know as the *Verhulst equation*, or *Verhulst-Pearl equation*), similar to density-dependent microbial turnover (Buchkowski et al., 2017; Georgiou et al., 2017). Using this formulation, the rate of change of the microbial population is determined by the size of

the population itself. At low population densities, the microbial community will grow unrestricted if sufficient substrate is available, while population growth will be more slowly when the population size approached a user-defined carrying capacity:

$$\frac{dP}{dt} = rP(1 - \frac{P}{K}) \tag{S8}$$

With *P* being the size of the population, *t* the time, *r* the growth rate per unit time and *K* the carrying capacity. In SOILcarb, the carrying capacity for microbes in the litter layer is defined as a fixed portion of total OC in the litter layer (K_{mic_L}, kg C m^{-2}). Re-writing eq. S8 for the rate of change of microbial biomass in the litter layer gives:

$$\frac{dC_{mic-l}}{dt} = r_l \cdot C_{mic-l}(1 - \frac{C_{mic-l}}{K_{mic-l}}) \tag{S9}$$

With r_l being the growth rate of microbial biomass in the litter layer (yr^{-1}), defined as the increase in C_{mic-l} as a portion of C_{mic-l}:

$$r_l = \frac{((F_{POC-l \to mic-l} \cdot \frac{1}{\alpha - 1}) + (F_{DOC-l \to mic-l} \cdot \frac{1}{\alpha - 1}))}{C_{mic-l}} \tag{S10}$$

The right-hand side of eq. S9 shows that the rate of microbial death per unit time (kg C m^{-2} yr^{-1}) can be formulated as:

$$death_{mic-l} = \frac{r_l \cdot C_{mic-l}^2}{K_{mic-l}} \tag{S11}$$

Dead microbial biomass is distributed over the C_{POC-l} and C_{DOC-l} pools as follows:

$$F_{C_{mic-l} \to C_{DOC-l}} = death_{mic-l} \cdot f_{sol} \tag{S12}$$

$$F_{C_{mic-l} \to C_{POC-l}} = death_{mic-l} \cdot (1 - f_{sol}) \tag{S13}$$

Where f_{sol} is the portion of microbial biomass that is soluble (unitless [0 - 1]).

S1.3.2 Litter OC loss through leaching and bioturbation

Bioturbation. The transfer of POC from the litter layer to the soil through bioturbation is simulated by transferring a portion of litter POC ($f_{bioturb}$, yr^{-1}) to the rhizosphere POC pool ($C_{POC\text{-}r}$) of the uppermost soil layer every time step:

$$F_{POC-l \to POC-r} = C_{POC-l} \cdot f_{bioturb} \tag{S14}$$

Where $f_{bioturb}$ is the fraction of the litter POC pool being transferred to the rhizosphere POC pool (yr^{-1}). Bioturbation of SOC is simulated as a diffusive process (Cousins et al., 1999; Gerino et al., 1994):

$$\frac{\partial C}{\partial t} = \frac{\partial}{\partial z}(D_b(z) \cdot \frac{\partial C}{\partial z}) \tag{S15}$$

Where C is the size of the carbon pool (kg C m^{-2}), t is the time (yr), z is the depth below the soil surface (m) and $D_b(z)$ is the biodiffusion coefficient (m^2 yr^{-1}) at depth z. The biodiffusion coefficient is assumed to decrease exponentially with depth (following Johnson et al. (2014)):

$$D_b(z) = D_b(0) \cdot e^{\frac{-z}{z_b}} \tag{S16}$$

Where $D_b(0)$ is the biodiffusion coefficient at the soil surface (z = 0) and z_b is the e-folding depth (m). In the current version of the model, the following SOC pools are bioturbated: $C_{POC\text{-}r}$, $C_{DOC\text{-}b}$, $C_{min\text{-}b}$ and $C_{min\text{-}b}$. Also the flux of POC and DOC from the litter layer into the soil are bioturbated before being added to $C_{POC\text{-}r}$ and $C_{DOC\text{-}b}$ respectively.

Leaching of litter DOC. Leaching of litter DOC to the soil is simulated by transferring a portion of the litter DOC pool ($C_{DOC\text{-}l}$) to the soil DOC pool ($C_{DOC\text{-}b}$) every time step. The amount of leached DOC from the litter layer (kg C m^{-2} yr^{-1}) is calculated as a fixed fraction of the size of the litter DOC pool:

$$F_{C_{DOC-l} \rightarrow C_{DOC-b}} = C_{DOC-l} \cdot f_{leach} \tag{S17}$$

Where f_{leach} is the portion of litter DOC inputs that is lost from the litter layer through leaching (yr^{-1}). This OC is added to the uppermost soil layer and subsequently advected downwards:

$$\frac{\partial C}{\partial t} = \nu \cdot \frac{\partial C}{\partial z} \tag{S18}$$

Where ν is the advection velocity (m yr^{-1}). The $C_{bioav\text{-}r}$ and $C_{DOC\text{-}b}$ are advected throughout the soil profile in the same way.

S1.3.3 Rhizosphere

Carbon inputs to the rhizosphere. OC inputs to the rhizosphere are divided into inputs through root exudates and dead roots (Figure S1). Total belowground OC inputs (i_{bg_tot}; kg C m^{-2} yr^{-1} down to 1 m depth) are divided into rhizosphere C inputs (F_{i_rhizo}; kg C m^{-2} yr^{-1}) and root C inputs (F_{i_root}; kg C m^{-2} yr^{-1}) as follows:

$$F_{i\_rhizo}(z) = f_{bg\_rhizo} \cdot i_{bg\_tot}(z) \tag{S19}$$

Where z is the depth (m) and f_{bg_rhizo} is the portion of total belowground carbon inputs that enters the soil as rhizodeposits (unitless). Carbon inputs as dead roots are calculated as:

$$F_{i\_root}(z) = (1 - f_{bg\_rhizo}) \cdot i_{bg\_tot}(z) \tag{S20}$$

Note that the in uppermost soil layer, the rhizosphere POC pools also receives OC inputs from bioturbated litter POC.

Belowground OC inputs are distributed over the depth profile using the following equation (Gale and Grigal, 1987; Jackson et al., 1996):

$$i_{bg\_cumul} = 1 - {\beta_r}^d \tag{S21}$$

Where i_{bg_cumul} is the cummulative root fraction ([0 – 1]) down to a depth d (cm) and β_r is a fitted coefficient (Jackson et al., 1996). Using this equation, the relative portion of total root inputs (i_{bg_tot}) is calculated for every soil layer.

Depolymerisation of POC. Particulate OC ($C_{POC\text{-}r}$) has to be depolymerized to become available for microbial uptake. This process is simulated using reverse Michaelis-Menten kinetics. For this formulation, the second term of the Michaelis-Menten equation is modified so that the rate of POC depolymerisation is modified based on the ratio of rhizosphere microbes to POC:

$$F_{C_{POC-r} \rightarrow C_{bioav-r}}(z) = V_{max,POC-r} \cdot C_{POC-r}(z) \cdot \frac{\frac{C_{mic-r}(z)}{C_{POC-r}(z)}}{K_{m,POC-r} + \frac{C_{mic-r}(z)}{C_{POC-r}(z)}} \tag{S22}$$

Where, $V_{max,POC-r}$ is the maximum depolymerisation rate (yr^{-1}), $K_{m,POC-r}$ is the ratio of C_{mic-r} to C_{POC-r} at which the maximum rate of depolymerisation is reduced by 50 % (unitless), C_{mic-r} is the amount of microbial biomass in the rhizosphere (kg C m^{-2} per depth layer) and C_{POC-r} is the amount of POC in the rhizosphere (kg C m^{-2} per depth layer) and z is the depth (m). The rate of depolymerisation of POC is modified by the ratio of C_{mic-r} to C_{POC-r} as it is the amount of microbes relative to the amount of POC, rather than the absolute amount of microbes, that determines the portion of POC that can potentially be depolymerised per time step.

Microbial uptake of bio-available carbon. The uptake of bio-available carbon in the rhizosphere ($C_{bioav\text{-}r}$), originating from rhizodeposits and depolymerised $C_{POC\text{-}r}$, is simulated using reversed Michaelis-Menten kinetics:

$$F_{C_{bioav-r} \rightarrow C_{mic-r}(z)} = V_{maxU,mic-r} \cdot C_{bioav-r}(z) \cdot \frac{\frac{C_{mic-r}(z)}{C_{bioav-r}(z)}}{K_{mU,mic-r} + \frac{C_{mic-r}(z)}{C_{bioav-r}(z)}} \cdot CUE\_r \cdot (1-\alpha) \tag{S23}$$

Where $V_{maxU,mic-r}$ is the maximum portion of $C_{bioav-r}$ that can be taken up by microbes per time step (yr^{-1}) and $K_{mU,mic-r}$ is the ratio of C_{mic-r} to $C_{bioav-r}$ at which the rate of uptake is reduced by 50 % (unitless), *CUE_r* is the carbon use efficiency in the rhizosphere (unitless) and α is the fraction of microbial C uptake obtained through heterotrophic CO_2 assimilation, which can be formulated as:

$$F_{CO_2 \rightarrow C_{mic-r}(z)} = V_{maxU,mic-r} \cdot C_{bioav-r}(z) \cdot \frac{\frac{C_{mic-r}(z)}{C_{bioav-r}(z)}}{K_{mU,mic-r} + \frac{C_{mic-r}(z)}{C_{bioav-r}(z)}} \cdot CUE\_r \cdot \alpha \tag{S24}$$

Microbial turnover. Similar to the litter layer, microbial turnover in the rhizosphere is simulated as a logistic growth process. The change in microbial carbon per time step can be written as:

$$\frac{\partial C_{mic-r}(z)}{\partial t} = F_{C_{bioav-r} \rightarrow C_{mic-r}}(z) + F_{CO_2 \rightarrow C_{mic-r}}(z) - death_{mic-r} \tag{S25}$$

Where z is depth below the soil surface (m), $F_{C_{bioav-r} \rightarrow C_{mic-r}}$ is microbial C uptake from bio-available C (kg C m^{-2} yr^{-1} per depth layer), $F_{CO_2 \rightarrow C_{mic-r}}$ is heterotrophic CO_2 assimilation (kg C m^{-2} yr^{-1} per depth layer) and $death_{mic-r}$ is the rate of microbial death (kg C m^{-2} yr^{-1} per depth layer), formulated as:

$$death_{mic-r} = \frac{r_r \cdot C_{mic-r}^2}{K_{mic-r}} \tag{S26}$$

Where K_{mic-r} is the carrying capacity for soil microbes in the rhizosphere, defined as a fixed portion of total organic carbon in the rhizosphere (i.e., the sum of C_{mic-r}, $C_{bioav-r}$ and C_{POC-r}; kg C m^{-2} per depth layer), and r_r is the relative growth rate of rhizosphere microbes (yr^{-1}):

$$r_r = \frac{F_{C_{bioav-r} \rightarrow C_{mic-r}(z)} \cdot \frac{1}{1-\alpha}}{C_{mic-r}} \tag{S27}$$

Upon death, microbial necromass is distributed over the bio-available carbon pool in the rhizosphere ($C_{bioav-r}$) and the DOC pool in the bulk soil (C_{DOC-b}):

$$F_{C_{mic-r} \rightarrow C_{bioav-r}}(z) = death_{mic-r} \cdot f_{sol} \tag{S28}$$

$$F_{C_{mic-r} \rightarrow C_{DOC-b}}(z) = death_{mic-r} \cdot (1 - f_{sol}) \tag{S29}$$

Where f_{sol} is the portion of microbial biomass that is soluble (unitless [0 – 1]).

S1.3.4 Bulk soil

Carbon inputs to the bulk soil. The bulk soil compartment of SOILcarb receives carbon from three source: (i) non-soluble necromass from microbes in the rhizosphere (Eq. S29), (ii) leached DOC from the litter layer (Eq. S17) and (iii) inputs from the bio-available C pool in the rhizosphere ($C_{bioav-r}$) to the soil DOC pool (C_{DOC-b}), to allow adsorption of plant-derived OC on soil minerals:

$$F_{C_{bioav-r} \rightarrow C_{DOC-b}}(z) = f_{bio \rightarrow DOC} \cdot C_{bioav-r}(z) \tag{S30}$$

Where $f_{bio \rightarrow DOC}$ (yr^{-1}) is the portion of $C_{bioav-r}$ that is transferred to the C_{DOC-b} pool per time step. It is noted that this portion is calculated on the remaining $C_{bioav-r}$ after C uptake by microbes in the rhizosphere (C_{mic-r}) have been subtracted.

Uptake of soil DOC by microbes and protection of OC in the bulk soil. In the bulk soil, there is competition for DOC (C_{DOC-b}) between microbes (for depolymerisation and microbial uptake, simulated in the bulk soil as a 1-step process) and minerals (C_{min-b}; for the protection of DOC from microbial uptake). Uptake and protection of DOC in the bulk soil are simulated using the equilibrium chemistry approximation (ECA) dynamics (Tang and Riley, 2013). Microbial depolymerisation

and subsequent uptake of C_{DOC-b} is simulated as:

$$F_{C_{DOC-b}\rightarrow C_{mic-b}}(z) = \frac{V_{max,DOC-b} \cdot C_{DOC-b}(z) \cdot C_{mic-b}(z)}{K_{m\_DOC-b} \cdot (1 + \frac{surf(z)}{K_{m\_ads}} + \frac{C_{mic-b}(z)}{K_{m\_DOC-b}}) + C_{DOC-b}(z)} \cdot (1-\alpha) \cdot CUE\_b \quad \text{(S31)}$$

Where $V_{max,DOC-b}$ is the maximum rate of depolymerisation and uptake (yr^{-1}), K_{m_DOC-b} is the affinity parameter for carbon depolymerisation and uptake by microbes (kg C m^{-3}; during model optimization, this parameter was defined as a % of TOC. Based on the soil mass per layer, this variable was then converted to kg OC m^{-2} per depth layer to be used for the different soil layers of the simulated depth profile), K_{m_ads} is the affinity parameter for adsorption of bulk soil DOC onto soil mineral surfaces (kg C m^{-3}; same remark as for K_{m_DOC-b}), $surf$ is the available surface area on soil minerals, expressed as the amount of OC that can be adsorbed (kg C m^{-3}), CUE_b the carbon use efficiency in the bulk soil (unitless) and α is the fraction of microbial carbon uptake through heterotrophic CO_2 fixation (unitless).

The amount of heterotrophic CO_2 assimilation by microbes in the bulk soil can thus be formulated as:

$$F_{CO_2\rightarrow C_{mic-b}}(z) = \frac{V_{max,DOC-b} \cdot C_{DOC-b}(z) \cdot C_{mic-b}(z)}{K_{m\_DOC-b} \cdot (1 + \frac{surf(z)}{K_{m\_ads}} + \frac{C_{mic-b}(z)}{K_{m\_DOC-b}}) + C_{DOC-b}(z)} \cdot \alpha \cdot CUE\_b \quad \text{(S32)}$$

Adsorption of soil DOC onto mineral surfaces (C_{min-b}) is simulated as:

$$F_{C_{DOC-b}\rightarrow C_{min-b}}(z) = \frac{V_{max,ads} \cdot C_{DOC-b}(z) \cdot surf(z)}{K_{m\_ads} \cdot (1 + \frac{surf(z)}{K_{m\_ads}} + \frac{C_{mic-b}(z)}{K_{m\_DOC-b}}) + C_{DOC-b}(z)} \quad \text{(S33)}$$

Where $V_{max,ads}$ is the maximum rate of adsorption of DOC onto mineral surfaces (yr^{-1}). The maximum amount of mineral-associated carbon ($C_{min-max}$) is defined following Georgiou et al. (2022). The amount of available surfaces for adsorption of OC is then defined as:

$$surf(z) = C_{min-max}(z) - C_{min-b}(z) \quad \text{(S34)}$$

As the amount of roots decreases with depth, and thus the amount of soil that is directly affected by roots, the variable $surf$ in Eq. S31, S32 and S33 is multiplied by the fraction of the soil volume occupied by the rhizosphere, as described in section S1.5.

De-protection of OC in the bulk soil. De-protection of mineral-associated OC (MAOC) is simulated as a first-order process:

$$F_{C_{min-b}\rightarrow C_{DOC-b}}(z) = k_{deprotect}(z) \cdot C_{min-b} \quad \text{(S35)}$$

Where $k_{deprotect}(z)$ is the rate at which MAOC is lost from soil minerals per time step (yr^{-1}) at depth z:

$$k_{deprotect}(z) = k_{deprotect}(0) \cdot f_{rhizo}(z) \quad \text{(S36)}$$

Where $k_{deprotect}(0)$ is the maximum value of $k_{deprotect}$ at the soil surface (z = 0) and $f_{rhizo}(z)$ (unitless) is the fraction of soil occupied by the rhizosphere at depth z (see section S1.5). The rate of MAOC desorption thus decreases as the volume of

soil occupied by the rhizosphere decreases, as it has been shown that root exudates enhance desorption of MAOC in the soil (Keiluweit et al., 2015)

Microbial turnover in the bulk soil. Similar to the other simulated soil compartments, microbial turnover in the bulk soil is simulated as a logistic growth process. The change in microbial OC per time step can be written as:

$$\frac{\partial C_{mic-b}(z)}{\partial t} = F_{C_{DOC-b}\rightarrow C_{mic-b}}(z) + F_{CO_2\rightarrow C_{mic-b}}(z) - death_{mic-b} \tag{S37}$$

Where $F_{C_{DOC-b}\rightarrow C_{mic-b}}(z)$ is the depolymerisation of C_{DOC-b} and subsequent uptake by microbes, $F_{CO_2\rightarrow C_{mic-b}}$ is heterotrophic CO_2 assimilation, and $death_{mic-b}$ is the rate of microbial death (kg C m^{-2} yr^{-1} per depth layer), formulated as:

$$death_{mic-b} = \frac{r_b \cdot C_{mic-b}^2}{K_{mic-b}} \tag{S38}$$

Where K_{mic-b} is the carrying capacity for soil microbes in the bulk soil, defined as a fixed portion of total organic carbon in the bulk soil (i.e., the sum of C_{mic-b}, C_{DOC-b} and C_{min-b}; kg C m^{-2} per depth layer), and r_b is the relative growth rate of bulk soil microbes (yr^{-1}):

$$r_b = \frac{F_{C_{DOC-b}\rightarrow C_{mic-b}}(z) \cdot \frac{1}{1-\alpha}}{C_{mic-b}} \tag{S39}$$

Upon microbial death, microbial biomass is transferred back to the C_{DOC-b} pool:

$$F_{C_{mic-b}\rightarrow C_{DOC-b}} = death_{mic-b} \tag{S40}$$

S1.4 Simulation of soil $^{13}CO_2$ and $^{14}CO_2$ depth profiles

To simulate the δ^{13}C and Δ^{14}C value of microbes after heterotrophic CO_2 assimilation along the soil depth profile, the δ^{13}C and Δ^{14}C value of soil CO_2 is simulated, using the mass balance equation of CO_2 in a one-dimensional diffusive medium based on Fick's first law (Amundson and Davidson, 1990; Cerling, 1984; Goffin et al., 2014):

$$\frac{\partial \epsilon(z)[CO_2]}{\partial t} = D_s(z)\frac{\partial^2[CO_2]}{\partial z^2} + P(z) \tag{S41}$$

Where ϵ is the air-filled soil porosity (m^3 m^{-3}), $[CO_2]$ is the CO_2 concentration, D_s is the effective soil diffusivity coefficient (m^2 yr^{-1}), t is the time (d) and P is the amount of CO_2 production per depth layer (μmol CO_2 m^{-3} d^{-1}). As soil hydrology is not simulated in the current version of SOILcarb, the air-filled porosity is assumed constant over time. The depth profile of air-filled porosity is assumed to exponentially decline from a user-defined value at the soil surface downwards:

$$\epsilon(z) = \epsilon(0) \cdot e^{(\frac{z}{z_e})} \tag{S42}$$

Where ϵ is the air-filled soil porosity (m^3 m^{-3}) at depth z (m), $\epsilon(0)$ is the air-filled porosity at the soil surface and z_e is the e-folding depth (m). The effective diffusivity of soil CO_2 (D_e; m^2 yr^{-1}) is calculated for undisturbed soils, following Moldrup

et al. (1997, 2000):

$$D_e(z) = D_0 \cdot 0.66 \cdot \epsilon(z) \cdot \left(\frac{\epsilon(z)}{\phi(z)}\right)^{\frac{12-m}{3}} \tag{S43}$$

Where D_0 is the gas diffusivity of CO_2 in free air (m^2 yr^{-1}), $\phi(z)$ is the total soil porosity (m^3 m^{-3}) and m is a coefficient with a value of 3 for undisturbed soils (Moldrup et al., 1997). It is noted that this is the D_e parameter that will be used for $^{12}CO_2$, while D_e values for $^{13}CO_2$ and $^{14}CO_2$ are calculated below. The total soil porosity is calculated as:

$$\phi(z) = 1 - \frac{\rho_{soil}(z)}{\rho_{min}} \tag{S44}$$

Where $\rho_{soil}(z)$ is the soil bulk density (g cm^{-3}) at depth z and ρ_{min} the bulk density of soil minerals (g cm^{-3}), assumed to be 2.65 g cm^{-3}. The gas diffusivity of CO_2 in free air (D_0) for a pressure p (atm) and temperature T (K) is calculated following Massman (1998):

$$D_0 = D_{0,spt}\frac{p_0}{p}\left(\frac{T}{T_0}\right)^{\alpha} \tag{S45}$$

Where $D_{0,spt}$ is the gas diffusion coefficient for CO_2 in free air under standard temperature (T_0, 273.15 K) and pressure (p_0, 1 atm) ($1.385 \cdot 10^{-5}$ m^3 s^{-1}; Massman (1998); note that this variable is convert to the units m^3 yr^{-1} in the model) and α is a coefficient (1.81; Massman (1998))). The production of CO_2 along the soil profile ($P(z)$; kg CO_2 m^{-3} yr^{-1}) is calculated as the sum of autotrophic (root respiration; P_{root}; kg CO_2-C m^{-3} yr^{-1}) and heterotrophic CO_2 production (soil organic carbon mineralization; P_{soc}; kg CO_2-C m^{-3} yr^{-1}):

$$P(z) = P_{root}(z) + P_{SOC}(z) \tag{S46}$$

The rate of root respiration ($P_{root}(z)$) at depth z is calculated as a fixed fraction of root biomass:

$$P_{root}(z) = \alpha_{resp} \cdot i_{bg_tot}(z) \tag{S47}$$

Where α_{resp} resp is a scalar (yr^{-1} [0 – 1]) used to calculated to amount of root respiration based on the total root biomass inputs at depth z. The CO_2 produced from mineralized soil organic carbon is calculated as:

$$P_{SOC}(z) = F_{C_{bioav-r}\rightarrow C_{mic-r}}(z) \cdot \frac{(1-CUE\_r)}{CUE\_r} \cdot \frac{1}{1-\alpha} + F_{C_{DOC-b}\rightarrow C_{mic-b}}(z) \cdot \frac{(1-CUE\_b)}{CUE\_b} \cdot \frac{1}{1-\alpha} \tag{S48}$$

The simulation of the depth profiles of the concentration of the isotopologues $^{12}CO_2$, $^{13}CO_2$ and $^{14}CO_2$ is performed using the same equations. However, the diffusivity of the respective molecules is adjusted based on their molecular weight (e.g. Cerling et al. (1991)):

$$D_e(^{13}CO_2) = \frac{D_e(^{12}CO_2)}{1.0044} \tag{S49}$$

$$D_e(^{14}CO_2) = \frac{D_e(^{12}CO_2)}{1.0088} \tag{S50}$$

Because OC inputs and other processes are constant within any given year of simulation, calculations of depth profiles of the concentrations of $^{12}CO_2$, $^{13}CO_2$ and $^{14}CO_2$ are performed once per year, assuming steady state with constant inputs and outputs of carbon within a year. This was done using Eq. S41. Using the concentrations of the different CO_2 isotopologues along the depth profile, the $\delta^{13}C$ and $\Delta^{14}C$ values of soil CO_2 was calculated, which is used to determine the $\delta^{13}C$ and $\Delta^{14}C$ of CO_2–derived carbon that is taken up by soil microbes.

S1.5 Calculation of rhizosphere volume

In SOILcarb, the portion of soil occupied by the rhizosphere is used as a proxy to simulate the effect of root dynamics on the protection and de-protection of mineral-associated organic carbon (C_{min-b}) (e.g. Keiluweit et al. (2015)). The volume occupied by the rhizosphere is calculated following the calculations presented in Finzi et al. (2015). First, the cumulative distribution of fine root length (FRL; km m^{-3}) to 1 m depth is calculated (Jackson et al., 1997):

$$r(d) = 1 - \beta^d \tag{S51}$$

Where $r(d)$ is the cumulative fraction of roots above a depth d (cm) and β an estimated shape parameter, equal to the β value used for the depth distribution of roots (Eq. S21). From this distribution, the fraction of fine root length per 1 cm depth increments is calculated, and multiplied with the total length of fine roots ($L_{fineRootTot}$; km m^{-3}), which was derived from Jackson et al. (1997). This yields the total length of fine roots in every depth layer ($L_{root}(z)$; km), where z is the depth). Next, the cumulative root diameter for different root diameter classes (intervals of 0.02 mm to 2 mm) was estimated using a logistic function:

$$CRL = \frac{1}{1 + (\alpha_r \cdot e^{-\gamma_r \cdot rootD})} \tag{S52}$$

Where CRL is the cumulative root length for the root diameter classes (km m^{-3}), $rootD$ (intervals of 0.02 mm to 2 mm; mm). The parameters α_r (value of 75) and γ_r (value of 11) are chosen by Finzi et al. (2015) based on the assumption that 75 % of roots have a diameter < 0.5 mm (see Finzi et al. (2015) for details). From this, the fraction of fine root length in the different diameter classes was calculated (*fFRL*). In a next step, the distribution of fine root length in different root diameter classes was used to calculate volume of soil affected by root exudates. Here, Finzi et al. (2015) assumed that finer roots exudate more than larger roots. Therefore, the distance root exudates travel from the root surface is assumed to exponentially decline with root diameter, with a maximum travel distance of 2 mm:

$$d_{exudates} = 2 \cdot e^{-k_{ex} \cdot rootD} \tag{S53}$$

Where $d_{exudates}$ is the distance travelled by root exudates (mm) from roots with a diameter $rootD$ (see above; mm) and k_{ex} a factor representing the rate at which root exudate distance decreases with increasing root diameter (fixed at a value of 1.5 by Finzi et al. (2015)). Assuming roots are cylindrical, the volume occupied by roots and root exudates for 1 m of roots (V_{rhizo_1m}; cm^3 m^{-1}) can then be calculated as:

$$V_{rhizo\_1m} = \sum_{i=1}^{100} \left(100 \cdot f_{FRL}(i) \cdot \pi \cdot \left(\frac{rootD(i) + d_{exudates}(i)}{10} \right)^2 \right) \tag{S54}$$

Where $f_{FRL}(i)$ is the fraction of fine root length in root diameter class i ($rootD(i)$; cm) (unitless). The factor 10 is used to convert mm to cm, while the factor 100 represent a length of roots of 100 cm. To obtain the total volume occupied by the rhizosphere in every depth layer (V_{rhizo}), V_{rhizo_1m} was multiplied by the total root length in every depth layer ($r(d)$; see above). The fraction of the soil occupied by roots (f_{rhizo_volume}) is calculated by dividing the volume of the rhizosphere (V_{rhizo}) by the volume of soil (V_{soil}) in each layer:

$$f_{rhizo_volume}(z) = \frac{V_{rhizo}(z)}{V_{soil}(z)} \tag{S55}$$

Where $V_{soil}(z)$ (cm^3) is the volume of soil per soil layer at depth z.

S1.6 Calculations for carbon isotopes (δ^{13}C and Δ^{14}C)

S1.6.1 Calculation of isotopic values

Values of δ^{13}C and Δ^{14}C are calculated as follows:

$$\delta^{13}C = \left(\frac{\frac{^{13}C}{^{12}C}}{\frac{^{13}C}{^{12}C}_{std}} - 1 \right) \cdot 1000 \tag{S56}$$

Where $\delta^{13}C$ is the δ^{13}C value of the soil organic carbon (‰), $\frac{^{13}C}{^{12}C}$ is the ratio of ^{13}C to ^{12}C of the sample and $\frac{^{13}C}{^{12}C}_{std}$ is the ratio of ^{13}C to ^{12}C for the PDB standard (0.0112372).

$$\Delta^{14}C = \left(\frac{\frac{^{14}C}{^{12}C}_{-25}}{0.95 \cdot \frac{^{14}C}{^{12}C}_{OX1,-19} \cdot e^{(\frac{(y-1950)}{8267})}} - 1 \right) \cdot 1000 \tag{S57}$$

Where $\frac{^{14}C}{^{12}C}_{-25}$ is the isotopic ratio of the sample, corrected as if it had a δ^{13}C value of -25 ‰, the second term in the denominator is an absolute standard that is decay-corrected for OX-I change since 1950 (see Schuur et al. (2016) for more information). The isotopic ratio of ^{14}C to ^{12}C normalized to a δ^{13}C of -25 ‰ ($\frac{^{14}C}{^{12}C}_{-25}$) is calculated as:

$$\frac{^{14}C}{^{12}C}_{-25} = \frac{^{14}C}{^{12}C}_{-[\delta]} \cdot \left[\frac{1 + (\frac{-25}{1000})}{1 + (\frac{\delta}{1000})} \right]^2 \tag{S58}$$

Where δ is the δ^{13}C value of SOC and $\frac{^{14}C}{^{12}C}_{-[\delta]}$ is the measured $\frac{^{14}C}{^{12}C}$ ratio. In SOILcarb, simulations are performed separately for the three isotopes ^{12}C, ^{13}C and ^{14}C. The distribution of total OC inputs over these three isotopes is calculated based on the δ^{13}C and Δ^{14}C values of inputs (from which the ratios of $\frac{^{13}C}{^{12}C}$ and $\frac{^{14}C}{^{12}C}$ can be obtained) as follows:

$$^{12}C = \frac{C_{tot}}{1 + \frac{^{13}C}{^{12}C} + \frac{^{14}C}{^{12}C}} \tag{S59}$$

$$^{13}C = (\frac{C_{tot}}{^{12}C} - \frac{^{14}C}{^{12}C} - 1) \cdot {}^{12}C \tag{S60}$$

$$^{14}C = C_{tot} - {}^{12}C - {}^{13}C \tag{S61}$$

S1.6.2 Processes affecting the isotopic values of carbon inputs over time

In the following sections, information is provided on how the δ^{13}C and Δ^{14}C values of plant biomass are calculated from the isotopic values of atmospheric CO_2, combined with the influence of atmospheric CO_2 concentration on the magnitude of isotopic discrimination of plants against ^{13}C and ^{14}C, relative to ^{12}C. The δ^{13}C and Δ^{14}C values of atmospheric CO_2 have substantial natural variations over time (Schmitt et al., 2012; Bauska et al., 2015) and have been greatly influenced by anthropogenic activity since the onset of the industrial revolution (Keeling, 1979). These variations have, in turn, affected the δ^{13}C and Δ^{14}C values of plant biomass (Keeling et al., 2017; Schubert and Jahren, 2012, 2015). To simulate the δ^{13}C and Δ^{14}C of carbon inputs to the soil over millenial timescales, multiple data sets have been compiled to obtain a continuous time series of the δ^{13}C and Δ^{14}C of atmospheric CO_2 for the period from 22,000 BCE (Before the Common Era) to 2015 CE (Common Era).

δ^{13}C of atmospheric CO_2. The data for the δ^{13}C value of atmospheric CO_2 has been compiled from Schmitt et al. (2012) for 22,000 BCE to 779 CE, from Bauska et al. (2015) for 780 to 1916 CE and from Graven et al. (2017) for 1917 to 2015 CE (Figure S4). When data was not available for every calendar year, linear interpolation was used to obtain annual data. The full times series of the δ^{13}C value of atmospheric CO_2 is shown in Figure S2.

Δ^{14}C of atmospheric CO_2. Data of the Δ^{14}C value of atmospheric CO_2 over the period 22,000 BCE to 2015 CE was obtained from the *IntCal13* dataset (Reimer et al., 2013) for the period 22,000 BCE to 1950 CE, and from Hua et al. (2013) for the period 1950 CE – 2009 CE. These data were obtained from the *SoilR* package in R (Sierra et al., 2014). Data for 2010 CE – 2015 CE were manually added from measurements performed at the Jongfraujoch measurement station (Switzerland), obtained from Hammer and Levin (2017). The combined data is presented in Figure S3.

Atmospheric CO_2 concentration. Data of atmospheric CO_2 concentration over the period 19,726 BCE to 2019 CE was obtained from Monnin (2006) for the period 19,726 BCE to 52 CE, from Meinshausen et al. (2017) for the period 53 CE – 2014 CE and from Keeling and Keeling (2017) for the period 2015 to 2019 CE. The combined data is presented in Figure 4.

S1.6.3 Isotopic values of leaf carbon inputs

The isotopic values of plant leaves ($\delta^{13}C_{leaf}$) is determined for every simulated year as follows:

$$\delta^{13}C_{leaf}(t) = \delta^{13}C_{atm}(t) - diff^{13}C_{atm-leaf}(t) \tag{S62}$$

Where $\delta^{13}C_{leaf}(t)$ is the δ^{13}C value of leaf biomass (‰) in calendar year *t*, $\delta^{13}C_{atm}(t)$ is the δ^{13}C value of atmospheric CO_2 in year *t* and $diff^{13}C_{atm-leaf}(t)$ is the difference in δ^{13}C between the atmosphere and leaves (‰). In SOILcarb, $diff^{13}C_{atm-leaf}(t)$ is calculated using a fixed and variable part. In the fixed part, the δ^{13}C value of plant material is a

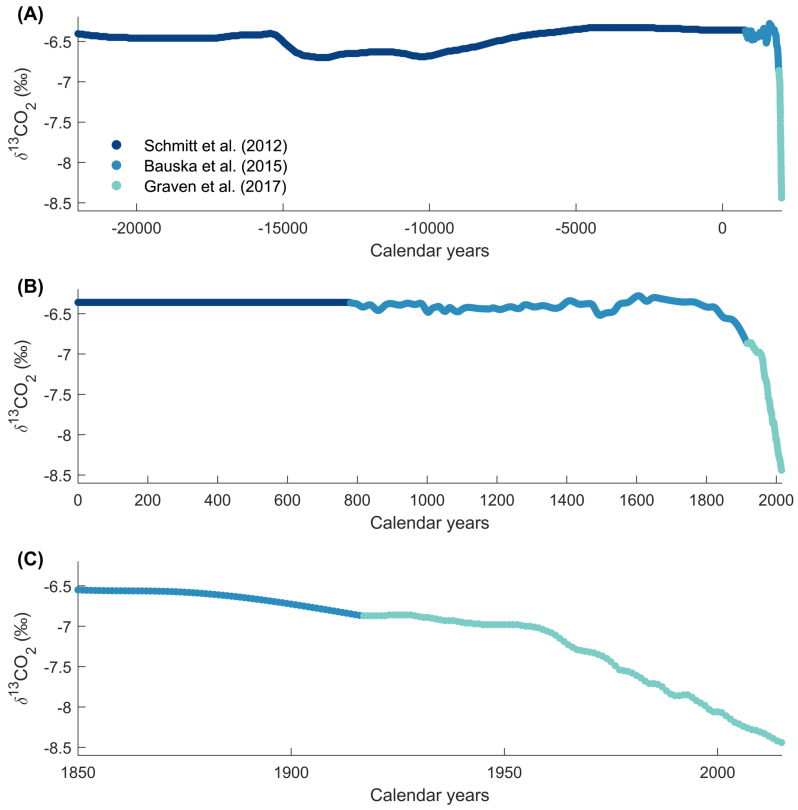

Figure S2. Compiled data of the δ^{13}C value of atmospheric CO_2 between 22,000 BCE to 2015 CE. (A), (B) and (C) show the same data, but for different periods of time, to illustrate the variation since the last glacial period (A), over the past two millennia (B) and the industrial period showing the ^{13}C Suess effect (C). Data sources: Schmitt et al. (2012) for 22,000 BCE (Before the Common Era) to 779 CE (Common Era), from Bauska et al. (2015) for 780 to 1916 CE and from Graven et al. (2017) for 1917 to 2015 CE.

function of changes in atmospheric $\delta^{13}CO_2$ through time (see section S1.6.2), with the magnitude of fractionation against ^{13}C during photosynthesis being constant through time. The fixed part is calculated using available data on the δ^{13}C value of plant leaves and the δ^{13}C value of atmospheric CO_2 for the last simulation year:

$$diff_{fixed} = \delta^{13}C_{atm}(t_{end}) - \delta^{13}C_{leaf}(t_{end}) \tag{S63}$$

Where $\delta^{13}C_{atm}(t_{end})$ is the δ^{13}C of atmospheric CO_2 during the last simulation year (*tend*) and $\delta^{13}C_{leaf}(t_{end})$ is the δ^{13}C value of leaves in the same year. We note that also measurement from any other simulation year can be used in these calculations. The variable part of $diff^{13}C_{atm-leaf}(t)$ is a function of the atmospheric CO_2 concentration, as it has been shown that the magnitude of fractionation against ^{13}C during photosynthesis increases with increasing atmospheric CO_2 concentrations in

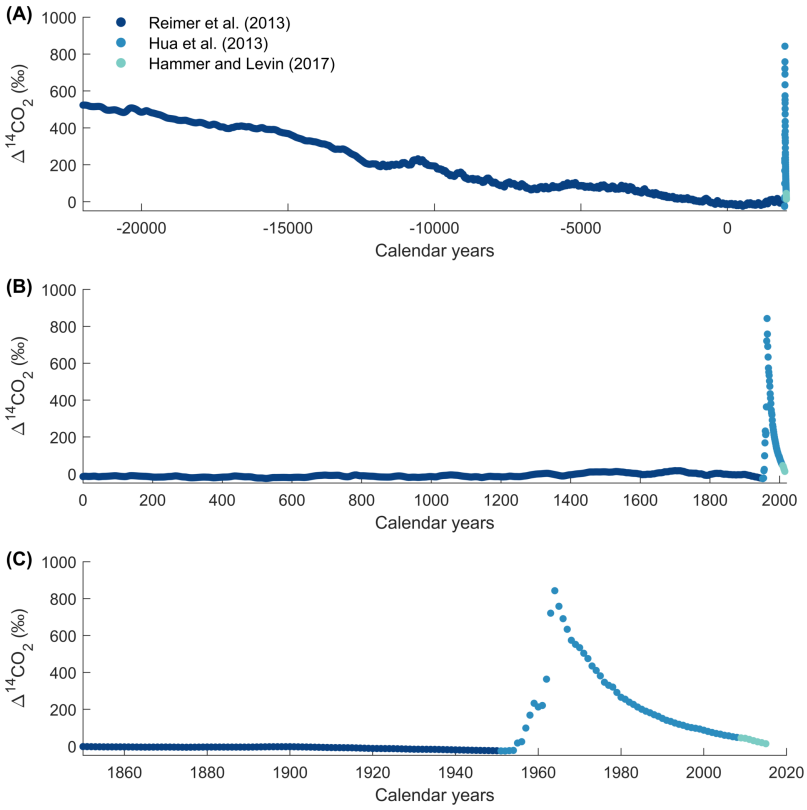

Figure S3. Compiled data of the $\Delta^{14}C$ value of atmospheric CO_2 between 22,000 BCE to 2015 CE. (A), (B) and (C) show the same data, but for different periods of time, to illustrate the variation since the last glacial period (A), over the past two millennia (B) and the industrial period showing the peak in 'bomb 14C' (C). Data sources: Reimer et al. (2013) for 22,000 BCE (Before the Common Era) to 1950 CE (Common Era), from Hua et al. (2013) for 1950 to 2009 CE and from Hammer and Levin (2017) for 2010 to 2015 CE.

C3 plants (Keeling et al., 2017; Schubert and Jahren, 2012, 2015):

$$diff_{variable}(t) = ([CO_2](t_{end}) - [CO_2](t)) \cdot S \tag{S64}$$

Where $[CO_2](t_{end})$ is the atmospheric CO_2 concentration (ppm) in the last simulated calendar year (*tend*), $[CO_2](t)$ is atmospheric CO_2 concentration in every other simulation year *t* and *S* represents the change in fractionation against ^{13}C by plants per unit change in atmospheric CO_2 concentration (‰ ppm^{-1}; Schubert and Jahren (2015)). This results in an increasing discrimination (i.e. more negative δ values) with increasing atmospheric CO_2 concentration. Combined, the factor $diff^{13}C_{atm-leaf}(t)$ is formulated as:

$$diff^{13}C_{atm-leaf}(t) = diff_{fixed} + diff_{variable}(t) \tag{S65}$$

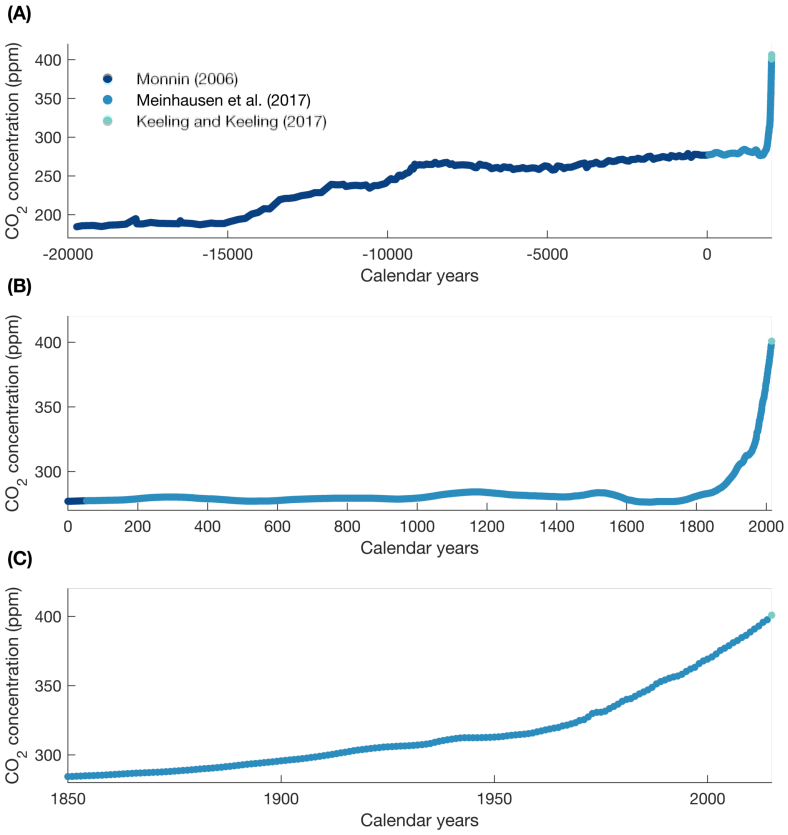

Figure S4. Compiled data of atmospheric CO_2 concentration between 19,726 BCE to 2019 CE. (A), (B) and (C) show the same data, but for different periods of time, to illustrate the variation since the last glacial period (A), over the past two millennia (B) and the industrial period showing the rapid increase in CO_2 concentration (C). Data sources: Monnin (2006) for 19,726 BCE (Before the Common Era) to 52 CE (Common Era), from Meinshausen et al. (2017) for 53 to 2014 CE and from Keeling and Keeling (2017) for 2015 to 2019 CE.

In contrast to δ^{13}C values, measurements of the Δ^{14}C value of plant biomass are generally not available. Therefore, the Δ^{14}C value of plant leaves is calculated by assuming that the magnitude of isotopic discrimination against ^{14}C during photosynthesis is twice that of against ^{13}C. This discrimination is calculated based on Eq. S56. This formula can be rewritten to obtain the ^{13}C/^{12}C ratio of the sample:

$$\frac{^{13}C}{^{12}C} = \left(\frac{\delta^{13}C}{1000} + 1\right) \cdot \frac{^{13}C}{^{12}C}_{std} \tag{S66}$$

The magnitude of isotopic discrimination during photosynthesis against ^{13}C can therefore be calculated as:

$$\Delta^{13}C_{atm-leaf} = \frac{\frac{^{13}C}{^{12}C}_{leaf}}{\frac{^{13}C}{^{12}C}_{atm}} \tag{S67}$$

Where $\Delta^{13}C_{atm-leaf}$ is the fractionation factor (unitless), $\frac{^{13}C}{^{12}C}_{leaf}$ is the isotopic ratio for leaves (unitless) and $\frac{^{13}C}{^{12}C}_{atm}$ is the isotopic ratio for atmospheric CO_2. Using this fractionation factor, the Δ^{14}C of leaves can be calculated as:

$$\Delta^{14}C_{leaf} = \Delta^{14}C_{atm} - 2 \cdot \Delta^{13}C_{atm-leaf} \tag{S68}$$

S1.6.4 Isotopic values of roots and root exudates

For C3 vegetation, roots are generally enriched in δ^{13}C compared to leaves, leading to a difference in δ^{13}C of 1 – 3 ‰ (Bowling et al., 2008; Ghashghaie and Badeck, 2014; Werth and Kuzyakov, 2010; Hobbie and Werner, 2004). The δ^{13}C value of roots ($\delta^{13}C_{root}$) is assumed to be enriched in ^{13}C compared to leaf biomass by a constant factor in all simulation years:

$$\delta^{13}C_{root} = \delta^{13}C_{leaf} + diff^{13}C_{leaf-root} \tag{S69}$$

Where $diff^{13}C_{leaf-root}$ (‰) is the difference in δ^{13}C value between leaves and roots (in the present study this value is 1.5 ‰). The Δ^{14}C value of roots ($\Delta^{14}C_{root}$) is calculated similar to the value for leaves by assuming that the magnitude of fractionation against ^{14}C between root biomass and atmospheric CO_2 is double than that for ^{13}C (see Eq. S68 and S69).

Root exudates are mainly derived from recently assimilated sugars through photosynthesis, with leaf sugars being enriched in δ^{13}C compared to bulk leaf material (Bowling et al., 2008). Therefore, the δ^{13}C value of root exudates ($\delta^{13}C_{exudates}$) is defined as a separate variable in the model. It is calculated based on a fixed different in the δ^{13}C value between leaves and root exudates ($diff^{13}C_{leaf-exudates}$; 0.4 ‰ in the present study). The Δ^{14}C value of root exudates ($\Delta^{14}C_{exudates}$) is calculated similar to the value for leaves by assuming that the magnitude of fractionation against ^{14}C between root exudates and atmospheric CO_2 is double than that for ^{13}C (see Eq. S68 and S69).

S2 Supplementary tables and figures

Table S1. Initial parameters selected for optimization. Parameters retained after the sensitivity analysis, and used to optimise the final model, are shown in bold. Lower and upper bound are the bounds between which the parameters were varied during the sensitivity analysis, selected as the ranges over which these parameters resulted in the 10 % best solutions during the initial model optimization. Note that K_{m_ads} and K_{m_DOC-b} have the units of %SOC [0 - 1], and are internally in the model converted to the unit kg C m^{-2} per depth layer, based on the depth profile of soil bulk density.

Parameter name	Lower bound	Upper bound
$\mathbf{D_b(0)}$	3.21E-5	9.97E-5
z_b	0.014	0.332
$\beta_\mathbf{r}$	0.851	0.909
$\mathbf{V_{max,POC-r}}$	0.696	0.905
$\mathbf{V_{maxU,mic-r}}$	0.011	0.998
$\mathbf{V_{max,ads}}$	243.8	999.5
$\mathbf{K_{m\_ads}}$	0.0133	0.291
$\mathbf{V_{max,DOC-b}}$	44.05	943.17
$\mathbf{K_{m\_DOC-b}}$	0.0582	0.999
$\mathbf{k_{deprotect}(0)}$	0.0328	0.269
ν	0.467	0.999

Table S2. Ranges between which the optimised model parameters were allowed to vary during optimisation. Note that K_{m_ads} and K_{m_DOC-b} have the units of %SOC [0 - 1], and are internally in the model converted to the unit kg C m^{-2} per depth layer, based on the depth profile of soil bulk density.

Parameter name	Lower bound	Upper bound
$\mathbf{V_{max,POC-r}}$	1E-2	1
$\mathbf{V_{maxU,mic-r}}$	1E-2	1
$\mathbf{D_b(0)}$	1E-8	1E-4
$\beta_\mathbf{r}$	0.85	0.97
$\mathbf{V_{max,ads}}$	1E-1	1E+3
$\mathbf{K_{m\_ads}}$	1E-8	1
$\mathbf{V_{max,DOC-b}}$	1E-1	1E+3
$\mathbf{K_{m\_DOC-b}}$	1E-6	1
$\mathbf{k_{deprotect}(0)}$	1E-6	1

Table S3. Optimal parameter values from the differential evolution algorithm for the four calibration scenarios. Note that K_{m_ads} and K_{m_DOC-b} have the units of %SOC [0 - 1], and are internally in the model converted to the unit kg C m^{-2} per depth layer, based on the depth profile of soil bulk density.

Parameter name	C	C and δ^{13}C	C and Δ^{14}C	C, δ^{13}C and Δ^{14}C
$\mathbf{V_{max,POC-r}}$	0.996	0.943	0.990	0.998
$\mathbf{V_{maxU,mic-r}}$	0.0952	0.743	0.981	0.856
$\mathbf{D_b(0)}$	1.03E-5	4.80E-6	1.95E-6	5.68E-6
$\beta_\mathbf{r}$	0.880	0.897	0.868	0.873
$\mathbf{V_{max,ads}}$	0.0906	0.0953	2.85E+2	2.89E+2
$\mathbf{K_{m\_ads}}$	0.676	4.49E-3	8.76E-3	0.155
$\mathbf{V_{max,DOC-b}}$	0.0513	3.28E-2	9.30E+2	1.12E+2
$\mathbf{K_{m\_DOC-b}}$	0.114	0.175	0.646	0.466
$\mathbf{k_{deprotect}(0)}$	3.67E-3	6.46E-1	1.18E-1	1.16E-1

Table S4. Parameters for which the sensitivity of the simulated δ^{13}C depth profile was assessed, and the ranges between which they were varied.

Parameter name	Lower bound	Upper bound
$\delta^{13}\mathbf{C_{leaf}}$	-29.9	-28.9
$\delta^{13}\mathbf{C_{root}}$	-28.3	-27.3
$\delta^{13}\mathbf{C_{exudates}}$	-29.4	-28.4
α	0	0.05
$\mathbf{S}$	0.0108	0.0172

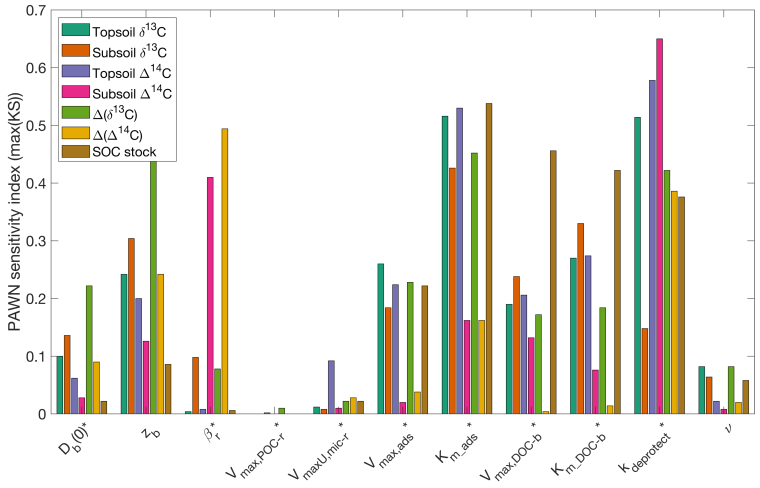

Figure S5. Results from the PAWN sensitivity analysis. The sensitivity index was calculated as the maximum of the Kolmogorov-Smirnov (KS) statistic, from which the value of a dummy variable has been subtracted. The sensitivity of multiple criteria to parameter variations was assessed: (1) *Topsoil* $\delta^{13}C$ (δ^{13}C at the soil surface), (2) *Subsoil* $\delta^{13}C$ (δ^{13}C at 0.4 m depth), (3) *Topsoil* $\Delta^{14}C$ (Δ^{14}C at the soil surface), (4) *Subsoil* $\Delta^{14}C$ (Δ^{14}C at 0.4 m depth), (5) $\Delta(\delta^{13}C)$ (the difference in δ^{13}C between the soil surface and 0.4 m depth), (6) $\Delta(\Delta^{14}C)$ (the difference in Δ^{14}C between the soil surface and 0.4 m depth) and (7) *SOC stock* (the total SOC stock). Parameters marked with an asterisk were retained for model optimisation.

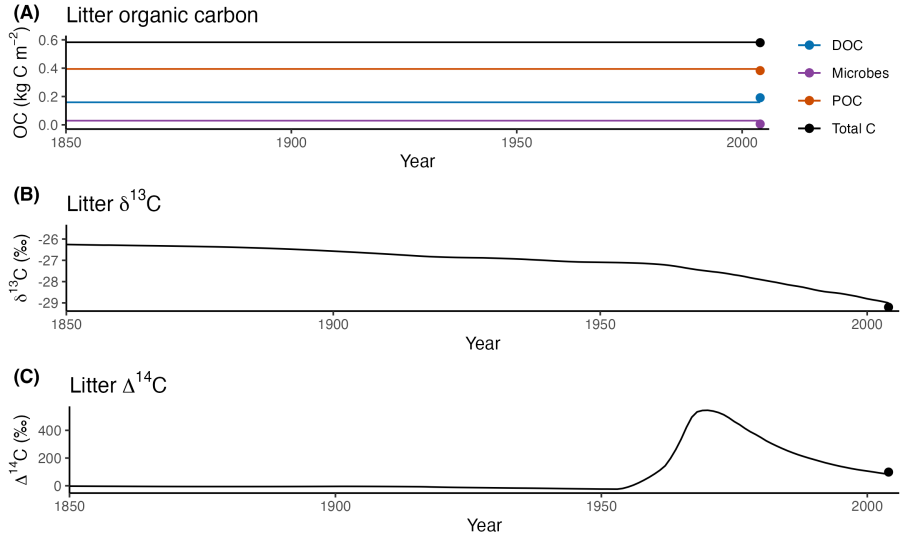

Figure S6. Result of simulations of litter OC pools for the period 1850 - 2004 after parameter optimisation based on OC, δ^{13}C and Δ^{14}C data: (A) total organic carbon, (B) δ^{13}C and (C) Δ^{14}C. Black dots denote measurements, with the portion of microbes, POC and DOC of litter C being based on assumptions.

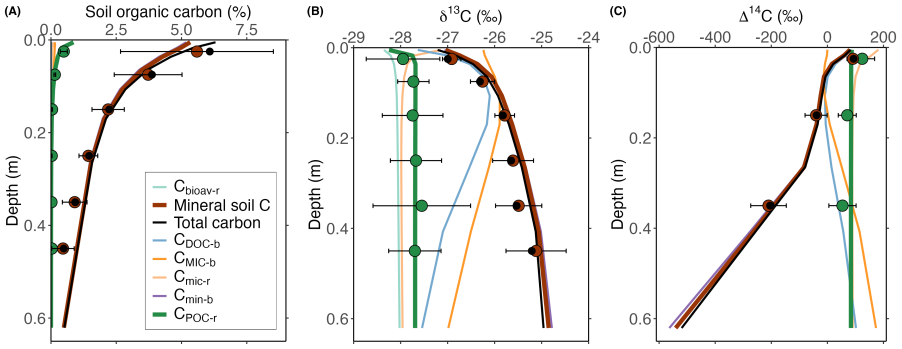

Figure S7. All simulated model pools in the year 2004 after parameter optimisation based on OC, $\delta^{13}C$ and $\Delta^{14}C$ data for (A) organic carbon, (B) $\delta^{13}C$ and (C) $\Delta^{14}C$. Dots denote measurements by Schrumpf et al. (2013).

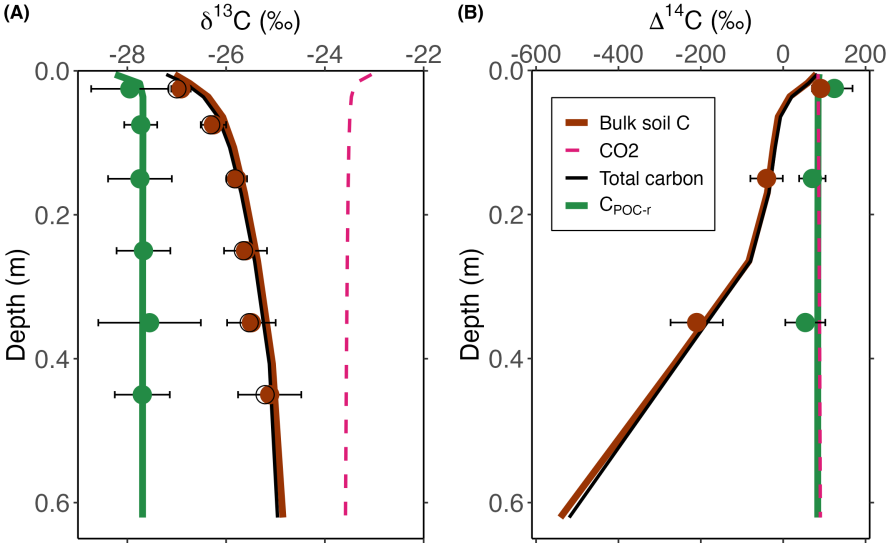

Figure S8. Simulated depth profiles of (A) $\delta^{13}C$ and (B) $\Delta^{14}C$ for model pools for which measured data were available, after the parameter optimisation based on OC, $\delta^{13}C$ and $\Delta^{14}C$. Simulated depth profiles of $\delta^{13}CO_2$ and $\Delta^{14}CO_2$ are shown in pink dashed lines. Dots denote measurements by Schrumpf et al. (2013).

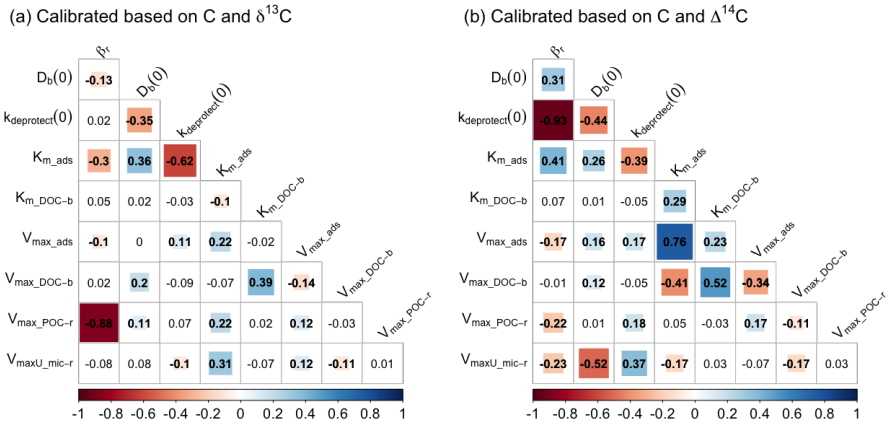

Figure S9. Correlation between the optimised parameters for the calibration scenarios using data on (A) OC and δ^{13}C and (B) OC and Δ^{14}C. Numbers are the Pearson correlation coefficients, while colors are shown for parameter combinations with a significant correlation ($p < 0.05$).

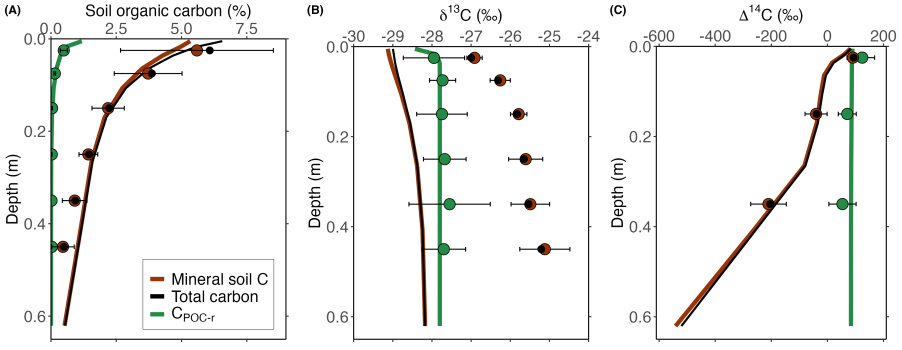

Figure S10. To quantify the effect of the mixing of OC derived from ^{13}C-depleted aboveground litter and ^{13}C-enriched root litter on the simulated depth profile of δ^{13}C, a model run was performed with this as the only mechanism influencing δ^{13}C along the soil profile. For this simulation, it was assumed that the δ^{13}C of atmospheric CO_2 was constant during the run, at the measured value for 2004. In addition, the effect of atmospheric CO_2 concentration on fractionation against ^{13}C during photosynthesis was turned off. Dots denote measurements by Schrumpf et al. (2013). Plots show the simulated depth profiles of (A) soil OC, (B) δ^{13}C and (C) Δ^{14}C.

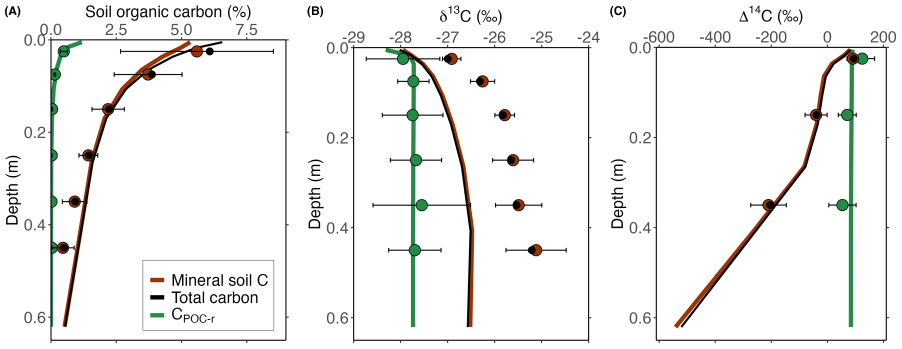

Figure S11. To quantify the effect of (i) the mixing of OC derived from ^{13}C-depleted aboveground litter and ^{13}C-enriched root litter and (ii) temporal changes in the δ^{13}C of vegetation (due to temporal variations in the δ^{13}C value of atmospheric CO_2) on the simulated δ^{13}C depth profile, a model run was performed with these as the only mechanisms influencing δ^{13}C along the soil profile. For this simulation, the effect of the atmospheric CO_2 concentration on fractionation against ^{13}C during photosynthesis was turned off. Dots denote measurements by Schrumpf et al. (2013). Plots show the simulated depth profiles of (A) soil OC, (B) δ^{13}C and (C) Δ^{14}C.

S3 Overview of state variables and model parameters

Table S5. State variables used in SOILcarb. *This parameter is calculated by subtraction the amount of mineral-associated OC ($C_{min\text{-}b}$) from the total amount of potential mineral-associated OC.

State variable	Description
Litter layer	
$C_{mic\text{-}l}$	Microbial biomass carbon in the litter layer
$C_{POC\text{-}l}$	Particulate organic carbon in the litter layer
$C_{DOC\text{-}l}$	Dissolvable organic carbon in the litter
Rhizosphere	
$C_{mic\text{-}r}$	Microbial biomass carbon in the rhizosphere
$C_{bioav\text{-}r}$	Bio-available carbon in the rhizosphere
$C_{POC\text{-}r}$	Particulate organic carbon in the rhizosphere
bulk soil	
$C_{mic\text{-}b}$	Microbial biomass carbon in the bulk soil
$C_{DOC\text{-}b}$	Dissolved OC in the bulk soil
$C_{min\text{-}b}$	Mineral-associated carbon in the bulk soil
*surf**	Available amount of mineral-associated carbon in the bulk soil

Table S6: Parameters used in SOILcarb. The calibrated values are shown in Table S3. Where possible, references to fixed values are provided in the detailed model description above.

Parameter	Unit	Description	Value
General parameters			
f_b	*Unitless*	Regulates increase in layer thickness with depth	0.5
α	*Unitless*	Fraction of microbial C uptake as CO_2	0.011
D_b	m^2 yr^{-1}	Biodiffusion coefficient	*Calculated*
$D_b(0)$	m^2 yr^{-1}	Biodiffusion coefficient at the soil surface	*Calibrated*
z_b	m	e-folding depth for the biodiffusion coefficient	0.15
ν	m yr^{-1}	Advection velocity of DOC in the soil	0.80
$\rho_{soil}(z)$	g cm^{-3}	Soil bulk density	*Provided by user*
Litter layer			
f_{leach}	yr^{-1}	Portion of annually leached DOC from the litter layer	0.20
$f_{bioturb}$	yr^{-1}	Portion of annually bioturbated POC from the litter layer	0.10
$f_{leachable}$	*Unitless*	Fraction leachable carbon of total litter inputs	0.4
i_{litter}	kg C m^{-2} yr^{-1}	Total amount of annual litter inputs	0.209
V_{max_POC-l}	yr^{-1}	Maximum depolimerisation of litter POC	95
V_{max_DOC-l}	yr^{-1}	Maximum depolimerisation of litter DOC	95
K_{m_POC-l}	kg C m^{-2}	Affinity for litter POC depolimerisation	7.15
K_{m_DOC-l}	kg C m^{-2}	Affinity for litter POC depolimerisation	3.53
CUE_l	*Unitless*	Carbon use efficiency of microbes in the litter layer	0.30
K_{mic-l}	kg C m^{-2}	Carrying capacity of microbes in the litter layer	0.05 * C_litter
f_{sol}	*Unitless*	Soluble portion of microbial necromass	0.5
Rhizosphere			
i_{bg_tot}	kg C m^{-2} yr^{-1}	Total belowground carbon inputs	0.322
f_{bg_rhizo}	*Unitless*	Portion of total belowground carbon inputs as rhizodeposits	0.29
β_r	*Unitless*	Extinction coefficient for root depth profile	*Calibrated*

Table S6: continued

Parameter	Unit	Description	Value
$f_{bio \rightarrow DOC}$	yr^{-1}	Fraction of bio-available C transferred to the soil DOC pool	0.175
$V_{max,POC-r}$	yr^{-1}	Maximum rate of rhizosphere POC depolimerisation	*Calibrated*
$K_{m,POC-r}$	*Unitless*	Half-saturation constant for rhizosphere POC depolimerisation	0.02
$V_{maxU,mic-r}$	yr^{-1}	Maximum rate of carbon uptake by rhizosphere microbes	*Calibrated*
$K_{mU,mic-r}$	*Unitless*	Half-saturation constant for C uptake by rhizosphere microbes	0.02
CUE_r	*Unitless*	Carbon use efficiency of rhizosphere microbes	0.30
K_{mic-r}	kg C m^{-2} per depth layer	Carrying capacity of microbes in the rhizosphere, as a portion of C in the rhizosphere	0.1 * C_rhizo
Bulk soil			
$V_{max,DOC-b}$	yr^{-1}	Maximum rate of carbon depolimerisation and uptake in the bulk soil	*Calibrated*
K_{m_DOC-b}	kg C m^{-3}	Affinity parameter for carbon depolimerisation and uptake by microbes in the bulk soil	*Calibrated*
$V_{max,ads}$	yr^{-1}	Maximum rate of adsorption of DOC onto mineral surfaces	*Calibrated*
K_{m_ads}	kg C m^{-3}	Affinity parameter for adsorption of soil DOC	*Calibrated*
CUE_b	*Unitless*	Carbon use efficiency of bulk soil microbes	0.30
$C_{min-max}$	kg C m^{-2} per depth layer	Maximum amount of mineral-associated carbon (note: 0.083 is calculated from Georgiou et al. (2022) for a soil with a sand content of 3 %)	0.083 * soil mass [kg C m^{-2} per depth layer]
$k_{deprotect}$	yr^{-1}	Rate of desorption of mineral-associated carbon	*Calibrated*
K_{mic-b}	kg C m^{-2} per depth layer	Carrying capacity of microbes in the bulk soil, as a portion of C in the bulk soil	0.03 * C_bulk
$^{13}CO_2$ and $^{14}CO_2$ depth profiles			
ϵ	m^3 m^{-3}	Air-filled soil porosity	*Calculated*

Table S6: continued

Parameter	Unit	Description	Value
$\epsilon(0)$	$m^3\ m^{-3}$	Air-filled porosity at the soil surface	0.2
z_e	m	e-folding depth of air-filled porosity	1
D_e	$m^2\ yr^{-1}$	Effective diffusivity of soil CO_2	*Calculated*
D_0	$m^2\ yr^{-1}$	Gas diffusivity of CO_2 in free air	*Calculated*
$D_{0,spt}$	$m^3\ s^{-1}$	Gas diffusion coefficient for CO_2 in free air under standard temperature (273.15 K) and pressure (1 atm)	$1.385 \cdot 10^{-5}$
ϕ	$m^3\ m^{-3}$	Soil porosity	*Calculated*
ρ_{min}	$g\ cm^{-3}$	Bulk density of soil minerals	2.65
m	-	Coefficient to calculate the effective gas diffusivity	3
T_0	K	Standard temperature	273.15 K
p_0	atm	Standard pressure	1
α	-	Coefficient to calculate gas diffusivity of OC_2 in free air	1.81
α_{resp}	yr^1	Fraction of root biomass respired as CO_2	0.5
Rhizosphere volume (from Finzi et al. (2015))			
f_{rhizo}	*Unitless*	Fraction of the soil occupied by the rhizosphere	*Calculated*
$r(d)$	-	Cumulative fraction of roots above a depth d (cm)	*Calculated*
$L_{fineRootTot}$	$km\ m^{-3}$	Total length of fine roots down to 1 m depth	5.4
L_{root}	$km\ m^{-2}$	Length of fine roots per cm depth interval	*Calculated*
CRL	$km\ m^{-2}$	Cumulative root length for the root diameter classes	*Calculated*
$rootD$	mm	Root diameter classes	-
α_r	-	Intercept	75
γ_r	mm^{-1}	Exponential decay constant	11
fFRL	-	Fraction of fine root length in the different diameter classes	*Calculated*
k_{ex}	mm^{-1}	Rate at which root exudate distance decreases with increasing root diameter	1.5
Calculations for $\delta^{13}C$ and $\Delta^{14}C$			
$\delta^{13}C_{leaf}$	‰	The $\delta^{13}C$ value of leaves	*Calculated*

Table S6: continued

Parameter	Unit	Description	Value
$diff^{13}C_{atm-leaf}(t)$	‰	The difference $\delta^{13}C$ between atmospheric CO_2 and leaves for simulation year *t*	*Calculated*
$diff_{fixed}$	‰	The fixed part in the difference in $\delta^{13}C$ between leaves and atmospheric CO_2	21.1
$diff_{variable}$	‰	The variable part in the difference in $\delta^{13}C$ between leaves and atmospheric CO_2	*Calculated*
S	‰ ppm^{-1}	Change in fractionation against ^{13}C by plants per unit change in atmospheric CO_2 concentration	0.014
$\delta^{13}C_{root}$	‰	The $\delta^{13}C$ value of roots	*Calculated*
$diff^{13}C_{leaf-root}$	‰	The difference in $\delta^{13}C$ values between leaves and roots	1.5
$\delta^{13}C_{exudates}$	‰	The $\delta^{13}C$ value of root exudates	*Calculated*
$diff^{13}C_{leaf-rhizodep}$	‰	The difference in $\delta^{13}C$ values between leaves and rhizodeposits	0.4

References

Akinyede, R., Taubert, M., Schrumpf, M., Trumbore, S., and Küsel, K.: Rates of dark CO2 fixation are driven by microbial biomass in a temperate forest soil, Soil Biology and Biochemistry, 150, 107 950, https://doi.org/10.1016/j.soilbio.2020.107950, 2020.

Amundson, R. G. and Davidson, E. A.: Carbon dioxide and nitrogenous gases in the soil atmosphere, Journal of Geochemical Exploration, 38, 13–41, https://doi.org/10.1016/0375-6742(90)90091-N, 1990.

Bauska, T. K., Joos, F., Mix, A. C., Roth, R., Ahn, J., and Brook, E. J.: Links between atmospheric carbon dioxide, the land carbon reservoir and climate over the past millennium, Nature Geoscience, 8, 383–387, https://doi.org/10.1038/ngeo2422, iSBN: 1752-0894, 2015.

Bowling, D. R., Pataki, D. E., and Randerson, J. T.: Carbon Isotopes in Terrestrial Ecosystem Pools and CO2 Fluxes, New Phytologist, 178, 24–40, https://doi.org/10.2307/30147703, iSBN: 0028646X, 2008.

Buchkowski, R. W., Bradford, M. A., Grandy, A. S., Schmitz, O. J., and Wieder, W. R.: Applying population and community ecology theory to advance understanding of belowground biogeochemistry, Ecology Letters, 20, 231–245, https://doi.org/10.1111/ele.12712, 2017.

Cerling, T. E.: The stable isotopic composition of modern soil carbonate and its relationship to climate, Earth and Planetary Science Letters, 71, 229–240, https://doi.org/10.1016/0012-821X(84)90089-X, 1984.

Cerling, T. E., Solomon, D. K., Quade, J., and Bowman, J. R.: On the isotopic composition of carbon in soil carbon dioxide, Geochimica et Cosmochimica Acta, 55, 3403–3405, https://doi.org/10.1016/0016-7037(91)90498-T, 1991.

Cousins, I. T., Mackay, D., and Jones, K. C.: Measuring and modelling the vertical distribution of semi-volatile organic compounds in soils. II: model development, Chemosphere, 39, 2519–2534, 1999.

Finzi, A. C., Abramoff, R. Z., Spiller, K. S., Brzostek, E. R., Darby, B. A., Kramer, M. A., and Phillips, R. P.: Rhizosphere processes are quantitatively important components of terrestrial carbon and nutrient cycles, Global Change Biology, 21, 2082–2094, https://doi.org/10.1111/gcb.12816, 2015.

Gale, M. R. and Grigal, D. F.: Vertical root distributions of northern tree species in relation to successional status, Canadian Journal of Forest Research, 17, 829–834, https://doi.org/10.1139/x87-131, iSBN: 9783540773405, 1987.

Georgiou, K., Abramoff, R. Z., Harte, J., Riley, W. J., and Torn, M. S.: Microbial community-level regulation explains soil carbon responses to long-term litter manipulations, Nature Communications, 8, 1–10, https://doi.org/10.1038/s41467-017-01116-z, publisher: Springer US, 2017.

Georgiou, K., Jackson, R. B., Vindušková, O., Abramoff, R. Z., Ahlström, A., Feng, W., Harden, J. W., Pellegrini, A. F. A., Polley, H. W., Soong, J. L., Riley, W. J., and Torn, M. S.: Global stocks and capacity of mineral-associated soil organic carbon, Nature Communications, 13, 3797, https://doi.org/10.1038/s41467-022-31540-9, publisher: Nature Publishing Group, 2022.

Gerino, M., Stora, G., and Durbec, J.-P.: Quantitative estimation of biodiffusive and bioadvective sediment mixing : In situ experimental approach, Oceanologica Acta, 17, 547–554, iSBN: 0399-1784, 1994.

Ghashghaie, J. and Badeck, F. W.: Opposite carbon isotope discrimination during dark respiration in leaves versus roots–a review, New Phytologist, 201, 751–769, iSBN: 1469-8137, 2014.

Goffin, S., Aubinet, M., Maier, M., Plain, C., Schack-Kirchner, H., and Longdoz, B.: Characterization of the soil CO2 production and its carbon isotope composition in forest soil layers using the flux-gradient approach, Agricultural and Forest Meteorology, 188, 45–57, https://doi.org/10.1016/j.agrformet.2013.11.005, publisher: Elsevier B.V., 2014.

Graven, H., Allison, C. E., Etheridge, D. M., Hammer, S., Keeling, R. F., Levin, I., Meijer, H. A. J., Rubino, M., Tans, P. P., Trudinger, C. M., Vaughn, B. H., and White, J. W. C.: Compiled records of carbon isotopes in atmospheric CO 2 for historical simulations in CMIP6, Geoscientific Model Development, 10, 4405–4417, https://doi.org/10.5194/gmd-10-4405-2017, 2017.

Hammer, S. and Levin, I.: Monthly mean atmospheric d14CO2 at Jungfraujoch and Schauinsland from 1986 to 2016 [dataset], https://doi.org/10.11588/data/10100, 2017.

Hobbie, E. A. and Werner, R. A.: Intramolecular, compound-specific, and bulk carbon isotope patterns in C3 and C4 plants: a review and synthesis, New Phytologist, 161, 371–385, https://doi.org/10.1111/j.1469-8137.2004.00970.x, _eprint: https://onlinelibrary.wiley.com/doi/pdf/10.1111/j.1469-8137.2004.00970.x, 2004.

Hua, Q., Barbetti, M., and Rakowski, A. Z.: Atmospheric radiocarbon for the period 1950-2010, Radiocarbon, 55, 2059–2072, https://doi.org/10.2458/azu_js_rc.v55i2.16177, iSBN: 0033-8222lescape}, 2013.

Jackson, R. B., Canadell, J., Ehleringer, J. R., Mooney, H. A., Sala, O. E., and Schulze, E. D.: A global analysis of root distributions for terrestrial biomes, Oecologia, 108, 389 – 411, https://doi.org/10.1007/BF00333714, 1996.

Jackson, R. B., Mooney, H. A., and Schulze, E. D.: A global budget for fine root biomass, surface area, and nutrient contents, Proceedings of the National Academy of Sciences, 94, 7362–7366, https://doi.org/10.1073/pnas.94.14.7362, 1997.

Johnson, M. O., Mudd, S. M., Pillans, B., Spooner, N. A., Fifield, L. K., Kirkby, M. J., and Gloor, M.: Quantifying the rate and depth dependence of bioturbation based on optically-stimulated luminescence (OSL) dates and meteoric 10Be, Earth Surface Processes and Landforms, 39, 1188–1196, https://doi.org/10.1002/esp.3520, iSBN: 0197-9337, 2014.

Keeling, C. D.: The Suess effect: 13Carbon-14Carbon interrelations, Environment International, 2, 229–300, https://doi.org/10.1016/0160-4120(79)90005-9, iSBN: 0160-4120, 1979.

Keeling, R. F. and Keeling, C. D.: Scripps CO2 Program Data. UC San Diego Library Digital Collections, https://doi.org/https://doi.org/10.6075/J0542KSG, 2017.

Keeling, R. F., Graven, H. D., Welp, L. R., Resplandy, L., Bi, J., Piper, S. C., Sun, Y., Bollenbacher, A., and Meijer, H. A. J.: Atmospheric evidence for a global secular increase in carbon isotopic discrimination of land photosynthesis, Proceedings of the National Academy of Sciences, 114, 10 361 – 10 366, https://doi.org/10.1073/pnas.1619240114, iSBN: 1619240114, 2017.

Keiluweit, M., Bougoure, J. J., Nico, P. S., Pett-Ridge, J., Weber, P. K., and Kleber, M.: Mineral protection of soil carbon counteracted by root exudates, Nature Climate Change, 5, 588–595, https://doi.org/10.1038/nclimate2580, iSBN: 1758-678X, 2015.

Massman, W. J.: A review of the molecular diffusivities of H2O, CO2, CH4, CO, O3, SO2, NH3, N2O, NO, and NO2 in air, O2 and N2 near STP, Atmospheric Environment, 32, 1111–1127, https://doi.org/10.1016/S1352-2310(97)00391-9, 1998.

Meinshausen, M., Vogel, E., Nauels, A., Lorbacher, K., Meinshausen, N., Etheridge, D. M., Fraser, P. J., Montzka, S. A., Rayner, P. J., Trudinger, C. M., Krummel, P. B., Beyerle, U., Canadell, J. G., Daniel, J. S., Enting, I. G., Law, R. M., Lunder, C. R., O'Doherty, S., Prinn, R. G., Reimann, S., Rubino, M., Velders, G. J. M., Vollmer, M. K., Wang, R. H. J., and Weiss, R.: Historical greenhouse gas concentrations for climate modelling (CMIP6), Geoscientific Model Development, 10, 2057–2116, https://doi.org/10.5194/gmd-10-2057-2017, 2017.

Miltner, A., Richnow, H.-H., Kopinke, F.-D., and Kästner, M.: Assimilation of CO2 by soil microorganisms and transformation into soil organic matter, Organic Geochemistry, 35, 1015–1024, https://doi.org/10.1016/j.orggeochem.2004.05.001, iSBN: 0146-6380, 2004.

Moldrup, P., Olesen, T., Rolston, D. E., and Yamaguchi, T.: Modeling diffusion and reaction in soils: VII. Predicting gas and ion diffusivity in undisturbed and sieved soils, Soil Science, 162, 632 – 640, 1997.

Moldrup, P., Olesen, T., Gamst, J., Schjønning, P., Yamaguchi, T., and Rolston, D. E.: Predicting the Gas Diffusion Coefficient in Repacked Soil, Soil Science Society of America Journal, 64, 1588 – 1594, https://doi.org/10.2136/sssaj2000.6451588x, 2000.

Monnin, E.: EPICA Dome C high resolution carbon dioxide concentrations [dataset], https://doi.org/10.1594/PANGAEA.472488, 2006.

Nel, J. A. and Cramer, M. D.: Soil microbial anaplerotic CO2 fixation in temperate soils, Geoderma, pp. 170–178, https://doi.org/10.1016/j.geoderma.2018.08.014, publisher: Elsevier, 2019.

R Core Team: R: A Language and Environment for Statistical Computing, R Foundation for Statistical Computing, Vienna, Austria, https://www.R-project.org/, 2024.

Reimer, P. J., Bard, E., Bayliss, A., Beck, J. W., Blackwell, P. G., Ramsey, C. B., Buck, C. E., Cheng, H., Edwards, R. L., Friedrich, M., Grootes, P. M., Guilderson, T. P., Haflidason, H., Hajdas, I., Hatté, C., Heaton, T. J., Hoffmann, D. L., Hogg, A. G., Hughen, K. A., Kaiser, K. F., Kromer, B., Manning, S. W., Niu, M., Reimer, R. W., Richards, D. A., Scott, E. M., Southon, J. R., Staff, R. A., Turney, C. S. M., and Plicht, J. v. d.: Intcal13 and marine13 radiocarbon age calibration curves 0 – 50,000 years cal bp, Radiocarbon, 55, 1869–1887, https://doi.org/10.2458/rc.v51i4.3569, iSBN: 0033-8222, 2013.

Schmitt, J., Schneider, R., Elsig, J., Leuenberger, D., Lourantou, A., Chappellaz, J., Kohler, P., Joos, F., Stocker, T. F., Leuenberger, M., and Fischer, H.: Carbon Isotope Constraints on the Deglacial CO2 Rise from Ice Cores, Science, 336, 711–714, https://doi.org/10.1126/science.1217161, 2012.

Schrumpf, M., Kaiser, K., Guggenberger, G., Persson, T., Kögel-Knabner, I., and Schulze, E.-D.: Storage and stability of organic carbon in soils as related to depth, occlusion within aggregates, and attachment to minerals, Biogeosciences, 10, 1675–1691, https://doi.org/10.5194/bg-10-1675-2013, iSBN: 1726-4170, 2013.

Schubert, B. A. and Jahren, A. H.: The effect of atmospheric CO2 concentration on carbon isotope fractionation in C3 land plants, Geochimica et Cosmochimica Acta, 96, 29–43, https://doi.org/10.1016/j.gca.2012.08.003, publisher: Elsevier Ltd, 2012.

Schubert, B. A. and Jahren, A. H.: Global increase in plant carbon isotope fractionation following the Last Glacial Maximum caused by increase in atmospheric pCO2, Geology, 43, 435–438, https://doi.org/10.1130/G36467.1, 2015.

Schuur, E. A. G., Druffel, E., and Trumbore, S. E., eds.: Radiocarbon and Climate Change, Springer International Publishing, ISBN 978-3-319-25641-2, https://doi.org/10.1007/978-3-319-25643-6, 2016.

Sierra, C. A., Müller, M., and Trumbore, S. E.: Modeling radiocarbon dynamics in soils: SoilR version 1.1, Geoscientific Model Development, 7, 1919–1931, https://doi.org/10.5194/gmd-7-1919-2014, iSBN: 0171-8630, 2014.

Soetaert, K., Petzoldt, T., and Setzer, R. W.: Solving Differential Equations in R: Package deSolve, Journal of Statistical Software, 33, 1–25, https://doi.org/10.18637/jss.v033.i09, 2010.

Tang, J. Y. and Riley, W. J.: A total quasi-steady-state formulation of substrate uptake kinetics in complex networks and an example application to microbial litter decomposition, Biogeosciences, 10, 8329–8351, https://doi.org/10.5194/bg-10-8329-2013, publisher: Copernicus GmbH, 2013.

Werth, M. and Kuzyakov, Y.: 13C fractionation at the root–microorganisms–soil interface: A review and outlook for partitioning studies, Soil Biology and Biochemistry, 42, 1372–1384, https://doi.org/10.1016/j.soilbio.2010.04.009, iSBN: 0038-0717 Publisher: Elsevier Ltd, 2010.

Šantrůčková, H., Bird, M. I., Elhottová, D., Novák, J., Picek, T., Šimek, M., and Tykva, R.: Heterotrophic Fixation of CO2 in Soil, Microbial Ecology, 49, 218–225, https://doi.org/10.1007/s00248-004-0164-x, iSBN: 0959-9428, 2005.

Šantrůčková, H., Kotas, P., Bárta, J., Urich, T., Čapek, P., Palmtag, J., Alves, R. J. E., Biasi, C., Diáková, K., Gentsch, N., Gittel, A., Guggenberger, G., Hugelius, G., Lashchinsky, N., Martikainen, P. J., Mikutta, R., Schleper, C., Schnecker, J., Schwab, C., Shibis-

tova, O., Wild, B., and Richter, A.: Significance of dark CO2 fixation in arctic soils, Soil Biology and Biochemistry, 119, 11–21, https://doi.org/10.1016/j.soilbio.2017.12.021, iSBN: 0038-0717, 2018.